First-principles calculation of lattice thermal conductivity in crystalline phase change materials: GeTe, Sb2Te3, and Ge2Sb2Te5

Davide Campi, Lorenzo Paulatto, Giorgia Fugallo, Francesco Mauri, Marco Bernasconi

First-principles calculation of lattice thermal conductivity in crystalline phase change materials: GeTe, Sb_2Te_3, and $Ge_2Sb_2Te_5$

Davide Campi,[1,2,3] Lorenzo Paulatto,[4] Giorgia Fugallo,[4,5] Francesco Mauri,[6] and Marco Bernasconi[1,*]

[1]*Dipartimento di Scienza dei Materiali, Università di Milano-Bicocca, Via R. Cozzi 55, I-20125 Milano, Italy*

[2]*Theory and Simulation of Materials (THEOS), École Polytechnique Fédéral Lausanne, CH-1015 Lausanne, Switzerland*

[3]*National Center for Computational Design and Discovery of Novel Materials (MARVEL), École Polytechnique Fédéral Lausanne, 1015 Lausanne, Switzerland*

[4]*Universitè Pierre et Marie Curie-Paris 6, Centre National de la Recherche Scientifique, IMPMC-UMR7590, Case 115, 4 Place Jussieu, 75252 Paris Cedex 05, France*

[5]*Laboratoire des Solides Irradiés, École Polytechnique, 91128 Palaiseau Cedex, France*

[6]*Dipartimento di Fisica, Università di Roma La Sapienza, Piazzale Aldo Moro 5, I-00185 Roma, Italy*

(Received 14 October 2016; revised manuscript received 21 December 2016; published 24 January 2017)

Thermal transport is a key feature for the operation of phase change memory devices which rest on a fast and reversible transformation between the crystalline and amorphous phases of chalcogenide alloys upon Joule heating. In this paper we report on the *ab initio* calculations of bulk thermal conductivity of the prototypical phase change compounds $Ge_2Sb_2Te_5$ and GeTe in their crystalline form. The related Sb_2Te_3 compound is also investigated for the sake of comparison. Thermal conductivity is obtained from the solution of the Boltzmann transport equation with phonon scattering rates computed within density functional perturbation theory. The calculations show that the large spread in the experimental data on the lattice thermal conductivity of GeTe is due to a variable content of Ge vacancies which at concentrations realized experimentally can halve the bulk thermal conductivity with respect to the ideal crystal. We show that the very low thermal conductivity of hexagonal $Ge_2Sb_2Te_5$ of about 0.45 $W\,m^{-1}\,K^{-1}$ measured experimentally is also resulting from disorder in the form of a random distribution of Ge/Sb atoms in one sublattice.

DOI: 10.1103/PhysRevB.95.024311

I. INTRODUCTION

Chalcogenide alloys are attracting an increasing interest for their use in optical data storage [digital versatile disk (DVD)] and, more recently, in electronic nonvolatile memories [phase change memories (PCMs)] [1–5]. These applications rest on a fast and reversible transformation between the amorphous and crystalline phases upon heating. The two phases can be discriminated thanks to a large contrast in their electrical conductivity (in PCMs) and optical reflectivity (in DVDs). In PCM operation, readout of the cell resistance is performed at low bias. Programming the memory requires instead a relatively large current to heat up the active layer and to induce the phase change which can be either the melting of the crystal and subsequent amorphization or the recrystallization of the amorphous phase.

Thermal conductivity (κ) is a key property for PCM operation, as the set/reset processes strongly depend upon heat dissipation and transport [6]. Several experimental works reported on the measurements of the bulk thermal conductivity of the prototypical GeSbTe phase change alloys [6–9] and the related binary compounds GeTe [10–15] and Sb_2Te_3 [11,16]. These compounds have a relatively low lattice thermal conductivity in the crystalline phase which has been ascribed to a strong phonon scattering by disordered point defects.

In the case of cubic $Ge_2Sb_2Te_5$, which is the metastable structure the amorphous phase crystallizes into in PCM devices, disorder is present in the form of a random distribution of Ge/Sb atoms and 20% of vacancies in one sublattice of the rocksalt structure, the other being fully occupied by Te atoms. Disorder leads to a lattice thermal conductivity of $\kappa = 0.40\,W\,m^{-1}\,K^{-1}$ which is close to the value of 0.27 $W\,m^{-1}\,K^{-1}$ measured for the amorphous phase [9].

In trigonal GeTe, vacancies in the Ge sublattice are responsible for the large spread of the measured thermal conductivity over the wide range of values 0.1–4.1 $W\,m^{-1}\,K^{-1}$ [10–15].

The lattice thermal conductivity is very low (0.45 $W\,m^{-1}\,K^{-1}$) [9] also in the hexagonal phase of $Ge_2Sb_2Te_5$ (GST), the crystalline phase stable at normal conditions, in which the vacancy concentration is much lower than that of the cubic phase. In this latter case, disorder may arise from a partial random distribution of Sb/Ge atoms. Actually, the hexagonal phase of $Ge_2Sb_2Te_5$ has $P\bar{3}m1$ symmetry and nine atoms per unit cell in nine layers stacked along the c axis, but the distribution of atoms in the different layers is still a matter of debate in literature. Two different ordered sequences have been proposed, namely, the ordered stacking Te-Sb-Te-Ge-Te-Ge-Te-Sb-Te-Te-Sb- (Kooi structure) [17] and the ordered stacking Te-Ge-Te-Sb-Te-Sb-Te-Ge-Te-Te-Ge- (Petrov structure) [18]. Most recent diffraction measurements suggested, however, a disordered phase with Sb and Ge randomly occupying the same layer [19] which is also confirmed by transmission electron microscopy imaging of $Ge_2Sb_2Te_5$ nanowires [20].

In this paper, we quantify the effect of the different types of disorder (vacancies and Ge/Sb distribution) on the lattice conductivity of hexagonal $Ge_2Sb_2Te_5$ and trigonal GeTe by means of density functional calculations. Phonon dispersion relations and anharmonic force constants are computed within density functional perturbation theory (DFPT) [21,22]. Lattice thermal conductivity is then obtained from the variational

*Corresponding author: davide.campi@epfl.ch

solution of the Boltzmann transport equation introduced in Ref. [23]. For the sake of comparison we have also investigated thermal transport in crystalline Sb_2Te_3 which is structurally similar to $Ge_2Sb_2Te_5$ and for which the effect of disorder is marginal.

II. COMPUTATIONAL METHODS

Phonon dispersion relations were calculated by means of DFPT [21] as implemented in the QUANTUM-ESPRESSO suite of programs [24]. We used either the local density approximation (LDA) or the Perdew-Burke-Ernzerhof (PBE) [25] generalized gradient corrected approximation (GGA) to the exchange and correlation functional. Van der Waals (vdW) interactions, not accounted for in the GGA schemes, were also included within the scheme proposed by Grimme [26]. Norm conserving pseudopotentials with only the outermost s and p valence electrons were used. The spin-orbit interaction was neglected since it has been shown to have negligible effects on the structural and vibrational properties of GeTe [27]. The Kohn-Sham (KS) orbitals were expanded in a plane-wave basis up to a kinetic cutoff of 30 Ry. The Brillouin-zone (BZ) integration for the self-consistent electron density was performed over Monkhorst-Pack (MP) meshes [28].

Third-order anharmonic force constants have been computed within DFPT as described in Ref. [22]. In this approach the three-phonons anharmonic coefficients for three arbitrary wave vectors ($\mathbf{q}$,$\mathbf{q}$',$\mathbf{q}$") are computed by using the so-called $2n+1$ theorem as formulated in Ref. [29]. This scheme is presently implemented only for the LDA functional in the QUANTUM-ESPRESSO package. The anharmonic force constants are thus always computed at the LDA level. The choice of the other functionals affects the harmonic phonons and the equilibrium lattice parameters at which anharmonic force constants have been computed. As discussed later in Sec. III, the harmonic phonons mostly depend on the choice of the lattice parameters and little on the choice of the functional once the lattice parameters are fixed. We could expect that the anharmonic force constants behave similarly. The calculation of the LDA anharmonic force constant at the lattice parameters either experimental or optimized with the other functionals (PBE or PBE+vdW) thus provides the dependence of the LDA anharmonic force constants on the lattice parameters. Moreover, to obtain consistent anharmonic force constants at the LDA level, the internal positions have been relaxed with the LDA functional at the equilibrium lattice parameters optimized with the other different functionals. We have also checked that by computing the LDA anharmonic force constants with the atomic positions optimized with the other functionals the thermal conductivity changes by less than 5%.

Phonons and anharmonic force constants are then used to solve exactly the linearized Boltzmann transport equation (BTE) by means of the variational technique introduced in Ref. [23] which we refer to for all the details. This new scheme provides a full solution of the BTE beyond the most commonly used single mode phonon relaxation time approximation (SMA) which describes rigorously the depopulation of the phonon states but not the corresponding repopulation. The momentum-conserving character of the normal (N) processes gives rise to a conceptual inadequacy of the SMA description and its use becomes questionable in the range of low temperatures where the umklapp (U) processes are frozen out and N processes dominate the phonon relaxation. The exact solution of the BTE allowed us to conclude that the SMA actually provides a good approximation at room temperature for the lattice thermal conductivity of the phase change compounds we are interested in for which the Debye temperature is actually below 300 K.

The effect of disorder in the distribution of Sb/Ge atoms in $Ge_2Sb_2Te_5$ was included in the calculation of the lattice thermal conductivity by considering only the effect of the different mass. The disorder in either the Petrov or Kooi structures is thus accounted for by adding a rate of elastic phonon scattering from isotopic impurities according to Ref. [30] (Eqs. (9) and (10) in Ref. [23]). The presence of vacancies in the Ge/Sb sublattice was also included as an isotope impurity scattering with a mass change $\Delta M = 3\,M$ where M is the mass of the atom removed according to Ratsifaritana and Klemens [31]. The reliability of this approximation was validated for GeTe by means of nonequilibrium molecular dynamics simulations [32] as discussed later on.

III. RESULTS

A. GeTe

At normal conditions, GeTe crystallizes in the trigonal ferroelectric phase (space group $R3m$) [33,34]. This structure, with two atoms per unit cell, can be viewed as a distorted rocksalt geometry with an elongation of the cube diagonal along the [111] direction and an off-center displacement of the inner Te atom along the [111] direction giving rise to a 3+3 coordination of Ge with three short stronger bonds (2.84 Å) and three long weaker bonds (3.17 Å). In the conventional hexagonal unit cell of the trigonal phase, the structure can be also seen as an arrangement of GeTe bilayers along the c direction with shorter intrabilayer bonds and longer interbilayers bonds (see Fig. 1). The trigonal phase transforms experimentally into the cubic paraelectric phase (space group $Fm\bar{3}m$) above the Curie temperature of 705 K [36].

The structural parameters of the trigonal phase consist of the lattice parameter a, the trigonal angle α, and the internal

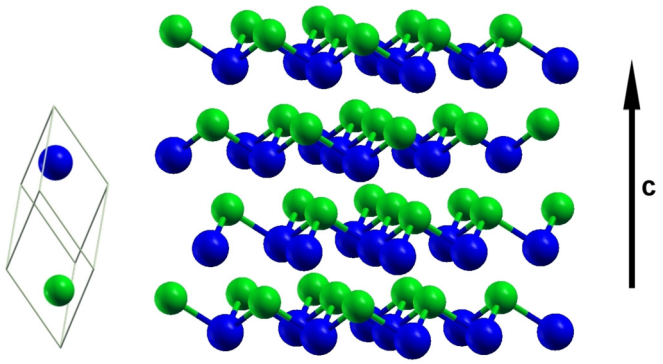

FIG. 1. Geometry of the GeTe crystal seen as a stacking of bilayers along the c axis of the conventional hexagonal unit cell with the three short intrabilayers bonds and three long interbilayers bonds. Green spheres denote Ge atoms and blue spheres denote Te atoms.

TABLE I. Structural parameters of the trigonal phase of crystalline GeTe computed within DFT with the LDA functional, the PBE functional with and without vdW interactions according to Grimme [26], and experimental data from Refs. [33,34]. The lengths of short and long bonds are also given.

Structural parameters	PBE	PBE +vdW	LDA	Exp.
a (Å)	4.33	4.22	4.23	4.31[a]–4.293[b]
α	58.14°	58.18°	58.79°	57.9°[a]–58.03°[b]
Unit-cell volume (Å^3)	54.98	51.75	52.00	53.88[a]–53.42[b]
x	0.2358	0.2380	0.2384	0.2366[a]–0.2357[b]
Short bond (Å)	2.85	2.82	2.83	2.84[a]–2.82[b]
Long bond (Å)	3.21	3.11	3.11	3.17[a]-3.18[b]

[a]Ref. [33].
[b]Ref. [34].

parameter x that assigns the positions of the two atoms in the unit cell, namely, Ge at (x,x,x) and Te at $(-x,-x,-x)$ [33]. The weaker interbilayer bonds may be seen as resulting from a partial resonant bonding between the short and long bond in a sort of three-centers-two-electrons bond. This idea, first proposed for GeTe by Lucovsky and White [35], was elaborated further in Ref. [37] to explain the optical contrast between the amorphous and crystalline states of phase change materials at large.

The theoretical structural parameters optimized at zero temperature with the PBE functional with or without vdW corrections are compared in Table I with the LDA results and the experimental data. The BZ integration for the self-consistent electron density was performed over a $12 \times 12 \times 12$ MP mesh. The equilibrium volume obtained with the PBE functional is very close to experiments while it is somehow underestimated with the LDA functional and the PBE functional plus vdW corrections.

Note that the addition of semiempirical vdW interaction according to Grimme to the PBE functional leads to a worse agreement with the experimental lattice parameters. This might be due to inaccuracies in the description of the damping of the vdW interaction at short distances and to the fact that the interbilayer bonding is not vdW-like but it is due to a partial resonant bonding as discussed above.

We remark that the theoretical equilibrium volume is computed at 0 K while the structural experimental data in Table I correspond to 300 K. An upper estimate of the total thermal expansion of the rhombohedral GeTe from 0 to 300 K can be obtained from the experimental volume thermal expansion coefficient at 300 K which equals 4.59 10^{-5} K^{-1} as obtained from neutron powder diffraction in Ref. [34]. This estimate yields $\Delta V/V$ of $4.59 \times 10^{-5} \times 300 = 1.38 \times 10^{-2}$, i.e., 1.38%, which is smaller than the difference between the experimental and theoretical volumes with all functionals in Table I.

The ideal GeTe crystal is a narrow gap semiconductor with a DFT-PBE band gap of 0.45 eV. It turns into a p-type degenerate semiconductor because of defects in stoichiometry, in the form of Ge vacancies, which induce the formation of holes in the valence band [38]. Hole concentrations are typically higher than 10^{19} holes/cm^3 in native p-type doped GeTe [39]. Higher

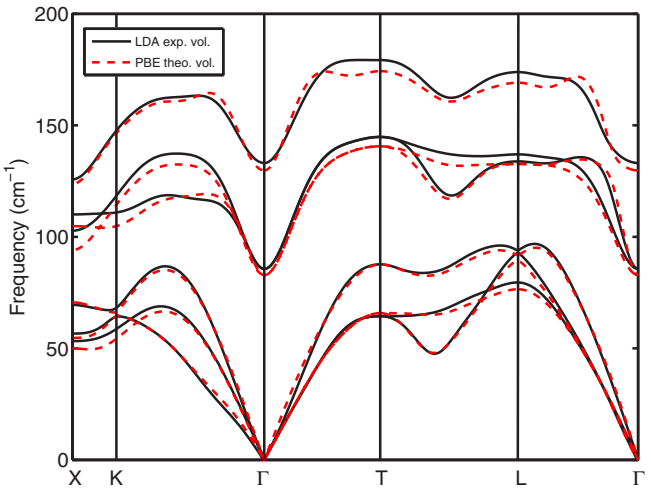

FIG. 2. Phonon dispersion relations of hole-doped GeTe (see text) from PBE calculations at the theoretical equilibrium lattice parameters and from LDA calculations at the experimental lattice parameters [33] (see Table I).

hole concentration of 1.6×10^{21} holes/cm^3 which corresponds to a vacancy content of about 4.3 at. % in the Ge sublattice (two holes per Ge vacancy) was also reported [27].

In the calculation of phonon dispersion relations we considered the presence of holes at the lower content of 8×10^{19} holes/cm^3 measured in Ref. [39], but at first we did not consider the presence of the companion Ge vacancies. We relaxed the atom positions by keeping the lattice parameters fixed at the values of the ideal crystal, which leads to a very small shift of the internal coordinate x to 0.2359 (for the PBE functional, see Table I). The Ge vacancies, present in the real crystal but lacking in our models of the p-type compound, are actually expected to affect the lattice parameters, as much as the holes in the valence bands do.

Phonons have been computed for the different functionals at the theoretical lattice parameters and for the LDA functional at the experimental lattice parameter [22] as well.

The results for the PBE functional at the theoretical lattice parameter and, for the LDA functional, at the experimental lattice parameters (close to the PBE ones) are compared in Fig. 2. The effect of holes on the phonon dispersions has been discussed in our previous work (with the PBE functional) [32] and in Ref. [27] (with the LDA functional), to which we refer to for further details. Different functionals yield very similar results once the calculations are performed with similar lattice parameters as it is the case for PBE and LDA phonons at the experimental lattice parameters. The same is true for PBE+vdW and LDA results at the theoretical lattice parameters. Conversely sizable differences are observed between the phonon dispersions computed with LDA at the theoretical and experimental lattice parameters and between the PBE and PBE+vdW phonons again due to a large change in the corresponding equilibrium volumes. All phonon dispersion relations have been obtained by Fourier interpolating the dynamical matrix computed in a $6 \times 6 \times 6$ MP grid in the BZ.

We then computed the lattice thermal conductivity for the ideal crystal at first without the effects of vacancies.

Anharmonic forces have been computed on a $4 \times 4 \times 4$ **q**-point phonon grid on the BZ, Fourier interpolated with a finer $15 \times 15 \times 15$ mesh for the BTE solution. Convergence was checked with a $25 \times 25 \times 25$ grid. Phonon energies have been broadened with a Gaussian function with smearing [40] of 2 cm^{-1} for energy conservation in three-phonon scattering processes. The anharmonic force constants were computed only with the LDA functional by optimizing the internal geometry with the lattice parameters fixed to the values used in the corresponding calculations of harmonic phonons (see Sec. II). This procedure leads to a small change in the short and long bonds below 0.3% (see Table I).

The resulting lattice thermal conductivity at 300 K computed with the exact variational solution of the BTE and PBE phonons along the z direction, parallel to the c axis in the hexagonal notation (see Fig. 1), is $\kappa_z = 2.00\,\mathrm{W m^{-1}\ K^{-1}}$ while the lattice thermal conductivity in the xy plane parallel to the GeTe bilayers (see Fig. 1) is $\kappa_x = 2.90\,\mathrm{W\,m^{-1}\ K^{-1}}$. For a polycrystalline sample the calculated average thermal conductivity is $\kappa_{\mathrm{av}} = \frac{2}{3}\kappa_x + \frac{1}{3}\kappa_z = 2.6\,\mathrm{W\,m^{-1}\ K^{-1}}$, which is an upper limit, as it neglects the effects of defects (vacancies in particular) and grain boundary scattering. κ_{av} is comparable to, although slightly larger than, the experimental value of $2.35 \pm 0.53\,\mathrm{W\,m^{-1}\,K^{-1}}$ of Ref. [10]. Including Grimme's van der Waals interaction in the phonons calculation at the theoretical lattice parameters leads to slightly higher thermal conductivities of $\kappa_z = 2.30\,\mathrm{W\,m^{-1}\ K^{-1}}$, $\kappa_x = 3.38\,\mathrm{W\,m^{-1}\ K^{-1}}$, and $\kappa_{\mathrm{av}} = 3.02\,\mathrm{W\,m^{-1}\ K^{-1}}$. By using the LDA functional for both the harmonic and anharmonic force constants at the experimental lattice parameters one obtains even larger lattice thermal conductivities of $\kappa_z = 2.37\,\mathrm{W\,m^{-1}\ K^{-1}}$, $\kappa_x = 3.62\,\mathrm{W\,m^{-1}\ K^{-1}}$, and $\kappa_{\mathrm{av}} = 3.20\,\mathrm{W\,m^{-1}\ K^{-1}}$.

Using the equilibrium Boltzmann distribution of phonons instead of the quantum Bose-Einstein distribution has no effect on the lattice thermal conductivity at 300 K (within the figures given here) due to the low Debye temperature (180 K). For the same reason the lattice thermal conductivities computed within the SMA are only slightly lower than the values obtained from the full solution of the BTE.

The lattice thermal conductivity within SMA is given by [23]

$$\kappa_x = \frac{1}{N_{\mathbf{q}} V_o} \sum_{\mathbf{q},j} C_{\mathbf{q},j} v^2_{\mathbf{q},j} \tau_{\mathbf{q},j} \qquad (1)$$

where the sum runs over the band index j and the $N_{\mathbf{q}}$ points in the BZ, $v_{\mathbf{q},j}$ is the group velocity along a generic coordinate x for band j at point $\mathbf{q}$, $C_{\mathbf{q},j}$ is the contribution to the specific heat of the $(\mathbf{q},j)$ phonon with frequency $\omega_{\mathbf{q},j}$ obtained from the derivative of the Bose-Einstein function f_{BE} with respect to temperature as $\hbar\omega_{\mathbf{q},j}\partial f_{\mathrm{BE}}(\omega_{\mathbf{q},j})/\partial T$, V_o is the unit-cell volume, and $\tau_{\mathbf{q},j}$ is the phonon lifetime obtained in turn from anharmonic force constants as discussed in Ref. [23] [see Eq. (B1) therein]. This approximation, when applicable, provides a more straightforward physical insight into the system, allowing one to account separately for each contributing factor to the thermal conductivity that appears in Eq. (1), and will be used with this purpose in the present paper after checking its validity by comparison with the exact BTE solution.

TABLE II. Lattice thermal conductivity (W m^{-1} K^{-1}) of ideal trigonal GeTe at 300 K along the c axis in the hexagonal notation (κ_z, see Fig. 1) in the perpendicular plane (κ_x) and their average for a polycrystalline sample (κ_{av}, see text), computed with the exact variational solution of the BTE and within the SMA. The PBE and PBE+vdW data refer to calculations at the theoretical equilibrium volumes. The LDA data refer to calculations at the experimental lattice parameters (see text).

	Exact			SMA		
	κ_z	κ_x	κ_{av}	κ_z	κ_x	κ_{av}
PBE	2.00	2.90	2.60	1.80	2.61	2.34
PBE+vdW	2.30	3.38	3.02	1.92	2.91	2.58
LDA	2.37	3.62	3.20	2.00	3.10	2.70

A summary of the resulting thermal conductivity computed with the different functionals and the comparison between the exact solution of the BTE and the SMA approximation are reported in in Table II.

The cumulative lattice thermal conductivity within the SMA of ideal trigonal GeTe as a function of phonons frequency is shown in Fig. 3 along with group velocities, phonon lifetimes, and mean free paths averaged over a small energy window of 2 cm^{-1}. The anharmonic broadening of the phonon branches computed as the inverse lifetime (Eq. (6) in Ref. [22]) within the SMA are also reported in Fig. 4. Another visualization of the anharmonic broadening is obtained by plotting the spectral function multiplied by the phonon frequency $\omega \cdot \sigma(\omega,\mathbf{q})$ shown in Fig. 5 where $\sigma(\omega,\mathbf{q})$

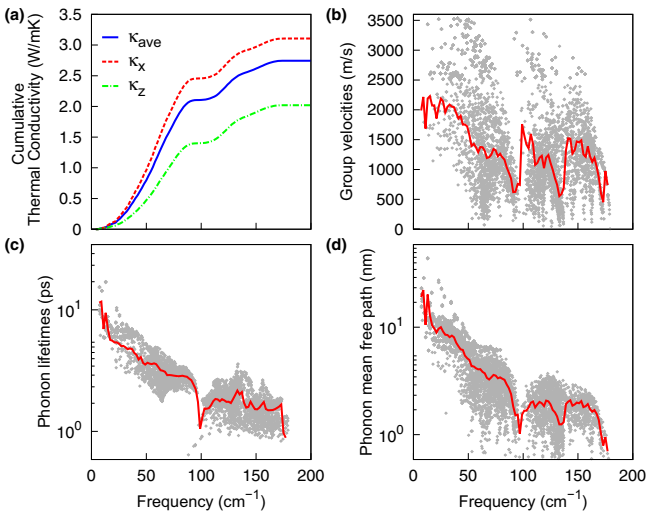

FIG. 3. (a) Cumulative lattice thermal conductivities within the SMA (see text) along the c axis in the hexagonal notation (κ_z, see Fig. 1) in the perpendicular plane (κ_x) and their average for a polycrystalline sample (κ_{av}, see text), (b) group velocities, (c) phonon lifetimes, and (d) mean free paths averaged over a small energy window of 2 cm^{-1} shown as a function of phonon frequencies in the ideal GeTe crystal (no vacancies) at 300 K. The data refer to LDA calculations at the experimental lattice parameters.

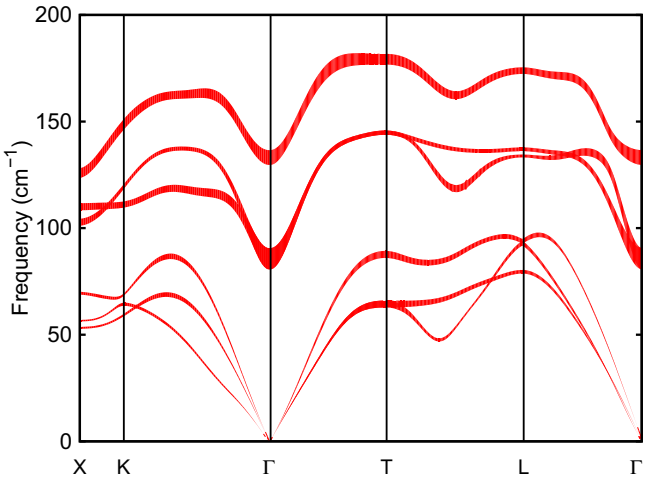

FIG. 4. Phonon dispersion relations of GeTe from LDA calculations at the experimental lattice parameters [33] (see Table I). The thickness of the curves corresponds to the anharmonic broadening computed as the inverse lifetime within the SMA.

is defined by [41]

$$\sigma(\mathbf{q},\omega) = \sum_j \frac{2\omega_{\mathbf{q},j}\tau^{-1}_{\mathbf{q},j}}{\left[\hbar^2\left(\omega^2 - \omega^2_{\mathbf{q},j}\right)\right]^2 + 4\hbar^2\omega^2_{\mathbf{q},j}\tau^{-2}_{\mathbf{q},j}}. \quad (2)$$

Comparison of Figs. 3(a) and 4 shows that the thermal conductivity is mostly due to acoustic phonons even at 300 K because of both low group velocities and lifetimes of optical phonons. All the data in Figs. 3–7 refer to LDA calculations at the experimental lattice parameters.

We then included the effects of vacancies in the Ge sublattice on the thermal conductivity by adding a rate of elastic scattering as due to isotopic defects in the BTE (see Sec. II). We considered two limiting vacancy contents of 0.2 at. % on the Ge sublattice corresponding to the hole concentration of 8×10^{19} holes/cm^3 studied experimentally in Ref. [39], and of 3 at. % that corresponds to a hole concentration of 1.1×10^{21} holes/cm^3 close to that studied experimentally in Ref. [27]. The lattice thermal conductivity (LDA phonons at the experimental lattice parameters and exact solution of the BTE) turns into $\kappa_z = 2.0\,\mathrm{W\,m^{-1}\,K^{-1}}$, $\kappa_x = 3.0\,\mathrm{W\,m^{-1}\,K^{-1}}$, and $\kappa_{\mathrm{av}} = 2.7\,\mathrm{W\,m^{-1}\,K^{-1}}$ for the low vacancy content or $\kappa_z = 0.9\,\mathrm{W\,m^{-1}\,K^{-1}}$, $\kappa_x = 1.4\,\mathrm{W\,m^{-1}\,K^{-1}}$, and $\kappa_{\mathrm{av}} = 1.2\,\mathrm{W\,m^{-1}\,K^{-1}}$ for the higher vacancy concentration to be compared with the values for the ideal GeTe of $\kappa_z = 2.37\,\mathrm{W\,m^{-1}\,K^{-1}}$, $\kappa_x = 3.62\,\mathrm{W\,m^{-1}\,K^{-1}}$, and $\kappa_{\mathrm{av}} = 3.20\,\mathrm{W\,m^{-1}\,K^{-1}}$ as given above. Even a small amount of Ge vacancies has thus a dramatic effect on the lattice thermal conductivity of GeTe which can be more than halved for 3 at. % in agreement with the experimental data in Ref. [15].

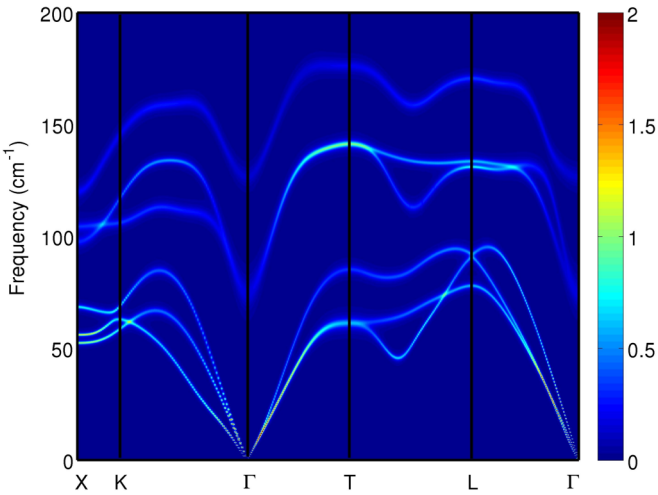

FIG. 5. Spectral function $\omega \cdot \sigma(\mathbf{q},\omega)$ [see Eq. (2)] of GeTe from LDA calculations at the experimental lattice parameters and only anharmonic broadening.

We remark that the effect of vacancies on the thermal conductivity has been actually introduced perturbatively as isotopic defects according to Ref. [31]. To assess the reliability of this approximation, we have performed nonequilibrium molecular dynamics (NEMD) simulations by using a highly transferable interatomic potential for GeTe obtained by fitting a large database of DFT-PBE energies with a neural network method [44]. The reliability of the classical approximation for phonons population at 300 K in GeTe, implicit in NEMD, has been demonstrated above. The NEMD simulations reported in Ref. [32] yield an average lattice thermal conductivity κ_{av} of 3.2 or 1.4 $\mathrm{W\,m^{-1}\,K^{-1}}$ for the ideal crystal or with 3 at. % of Ge vacancies. The reduction of the thermal conductivity due to vacancies is quantitatively similar to the results obtained from BTE, which yields 3.2 or 1.2 $\mathrm{W\,m^{-1}\,K^{-1}}$ for the ideal and defective (3% of vacancies) crystal (LDA phonons at the experimental lattice parameters). The good agreement between the NEMD and BTE results assesses the reliability of the approximation used to deal with Ge vacancies in the solution of the BTE. The cumulative lattice thermal conductivity and average phonon mean free path within the SMA is shown in Fig. 6 as a function of phonons frequency for trigonal GeTe with 3 at. % of Ge vacancies. These results have to be compared with the corresponding data for ideal GeTe in Fig. 3.

We further remark that in the presence of holes in the valence bands the phonon lifetimes can be reduced also by electron-phonon scattering processes. These effects are, however, negligible in GeTe at the doping levels discussed above. To estimate the reduction of thermal conductivity due to electron-phonon scattering we removed from the calculation of κ the contribution of all phonons with wave vector q smaller than twice the larger wave vector on the Fermi surface. This corresponds to a large overestimation of the effects of the electron-phonon coupling that, nevertheless, leads to a slight reduction of the thermal conductivities to $\kappa_z = 2.2\,\mathrm{W\,m^{-1}\,K^{-1}}$ and $\kappa_x = 3.1\,\mathrm{W\,m^{-1}\,K^{-1}}$.

Finally, we calculated the temperature dependence of the thermal conductivity in GeTe with 3% vacancies as reported in Fig. 7.

B. Sb_2Te_3

Crystalline Sb_2Te_3 has a rhombohedral geometry [$R\bar{3}m$ space group (D^5_{3d})] with five atoms per unit cell [42,43]. The crystal structure can be better visualized in the conventional

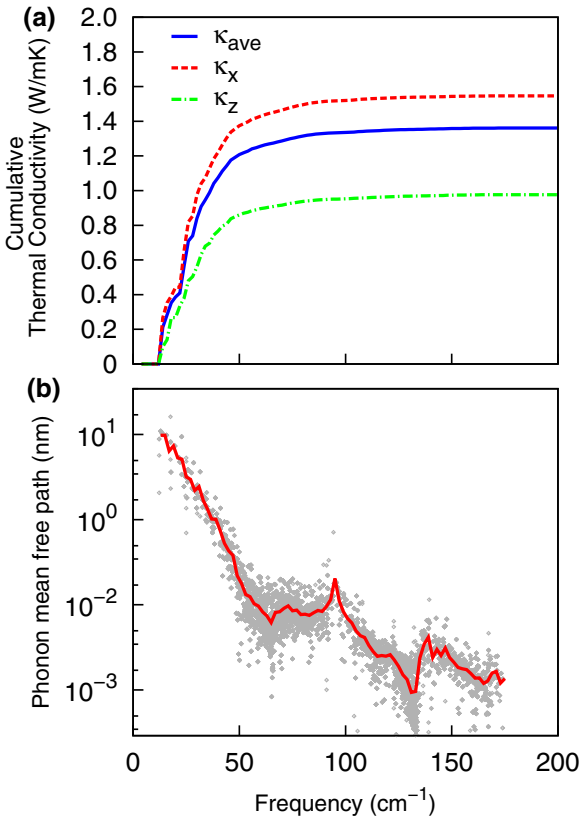

FIG. 6. (a) Cumulative lattice thermal conductivities within the SMA (see text) along the c axis in the hexagonal notation (κ_z, see Fig. 1) in the perpendicular plane (κ_x) and their average for a polycrystalline sample (κ_{av}, see text), and (b) mean free paths averaged over a small window of $2\,cm^{-1}$ as a function of phonon frequencies for GeTe with 3 at. % of Ge vacancies at 300 K. The data refer to LDA calculations at the experimental lattice parameters.

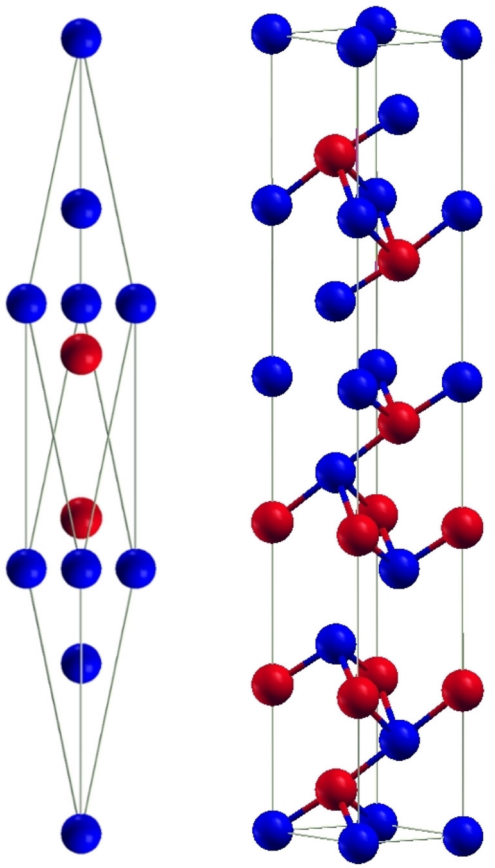

FIG. 8. Structure of Sb_2Te_3 in the unit rhombohedral cell and conventional hexagonal supercell (three formula units). Blue and red spheres denote Te and Sb atoms.

hexagonal supercell with three formula units (Fig. 8). In the hexagonal cell we recognize three slabs, each formed by five hexagonal layers stacked along c in the sequence Te-Sb-Te-Sb-Te, each layer containing a single atom in the unit cell. The weak Te-Te bonds, 3.736 Å long [42], connecting adjacent slabs are not shown in Fig. 8 to emphasize the presence of Sb_2Te_3 structural units. The three atoms independent by symmetry are at crystallographic positions Te1 = (0, 0, 0), Te2 = (0, 0, x), and Sb = (0, 0, y).

We computed the phonon dispersion relation of Sb_2Te_3 with the PBE functional in our previous work [45]. Here, we consider the PBE functional supplemented by the vdW corrections [26] to better reproduce the weak Te-Te interaction. The equilibrium structural parameters obtained with PBE and PBE+vdW functionals are compared in Table III with the experimental data [42]. Integration of the BZ for the self-consistent solution of the Kohn-Sham equation is performed over a $6 \times 6 \times 6$ MP mesh.

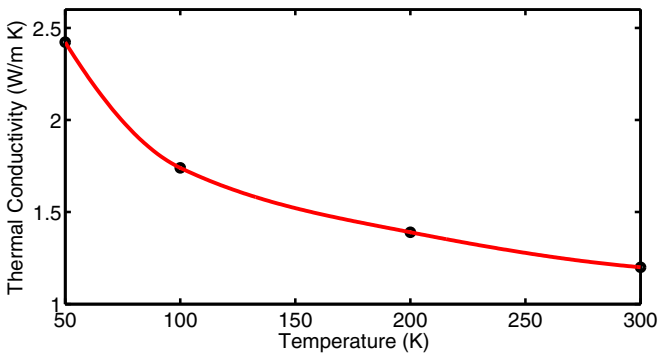

FIG. 7. Temperature dependence of thermal conductivity of polycrystalline GeTe with 3% of Ge vacancies. The data refer to LDA phonons at the experimental lattice parameters.

TABLE III. Structural parameters of crystalline Sb_2Te_3 from DFT calculations with the PBE or PBE+vdW functionals (see text) compared with the experimental data from Refs. [42,43].

Structural parameters	PBE	PBE+vdW	Exp.
a (Å)	4.316	4.219	4.264[a]–4.271[b]
c (Å)	31.037	30.692	30.458[a]–29.877[b]
x	0.785	0.786	0.787[a]
y	0.397	0.397	0.399[a]

[a]Ref. [42].
[b]Ref. [43].

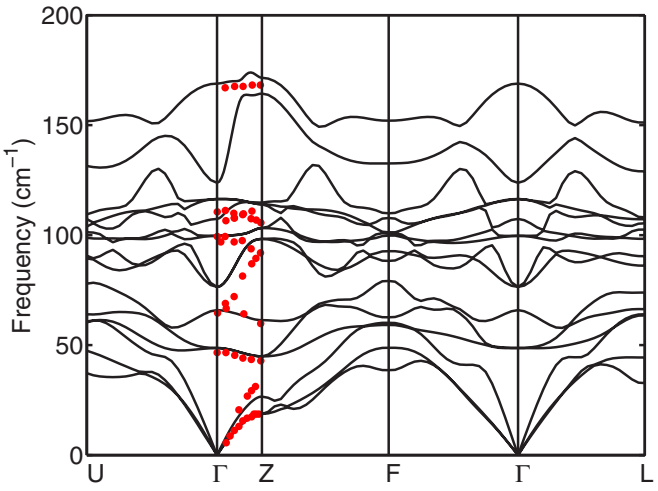

FIG. 9. Phonon dispersion relations of Sb_2Te_3 from PBE+vdW calculations. The dots are experimental data from neutron inelastic-scattering measurements at room temperature [46].

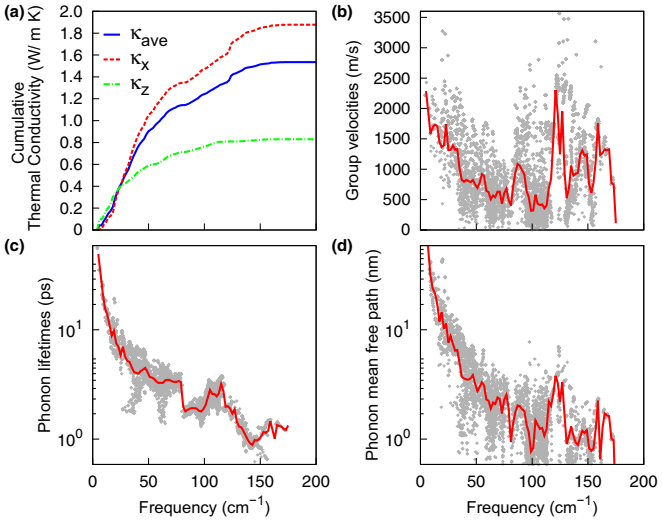

FIG. 10. (a) Cumulative lattice thermal conductivities within the SMA (see text) along the c axis in the hexagonal notation (κ_z, see Fig. 8) in the perpendicular plane (κ_x) and their average for a polycrystalline sample (κ_{av}, see text), (b) group velocities, (c) phonon lifetimes, and (d) mean free paths averaged over a small window of 2 cm^{-1} as a function of phonon frequencies in Sb_2Te_3 crystal at 300 K.

Experimentally this compound is a degenerate p-type semiconductor with a hole concentration of about 1.0×10^{20} holes/cm^3 possibly due to an Sb excess substituting Te [11]. As for the case of GeTe, we introduced holes in the valence bands compensated by a uniform negative background to ensure charge neutrality. The internal structure has been optimized by fixing the lattice parameters to those obtained without holes. Phonon dispersion relations have been obtained by Fourier transforming the dynamical matrix computed on a $6 \times 6 \times 6$ MP grid in the BZ.

The dispersion curves computed with PBE+vdW functionals at the theoretical equilibrium parameters are reported in Fig. 9 together with the available experimental data from neutron inelastic scattering [46].

Anharmonic force constants have been computed following the same scheme used for GeTe and discussed in the previous section. A $4 \times 4 \times 4$ q-point grid has been used. Fourier interpolation has been made over a $15 \times 15 \times 15$ grid with a smearing of 2 cm^{-1} for energy conservation.

The resulting lattice thermal conductivities at 300 K computed with PBE+vdW phonons and solving exactly the BTE are $\kappa_z = 0.8\,\mathrm{W\,m^{-1}\,K^{-1}}$, $\kappa_x = 2.0\,\mathrm{W\,m^{-1}\,K^{-1}}$, and $\kappa_{av} = 1.6\,\mathrm{W\,m^{-1}\,K^{-1}}$, which compares well with the experimental value of $\kappa_{av} = 1.3\,\mathrm{W\,m^{-1}\,K^{-1}}$ of Ref. [11] or $1.8\,\mathrm{W\,m^{-1}\,K^{-1}}$ of Ref. [16]. Also in this case the difference between the exact BTE solution and the SMA is rather small with a SMA thermal conductivity of $\kappa_z = 0.78\,\mathrm{W\,m^{-1}\,K^{-1}}$, $\kappa_x = 1.9\,\mathrm{W\,m^{-1}\,K^{-1}}$.

In our model of Sb_2Te_3 the sublattice is ordered, but we expect a fraction of about 0.76% of Te sites occupied by Sb atoms due to a hole concentration of 10^{20}/cm^2 [11]. This defects content could bring the slightly overestimated theoretical thermal conductivity to a better agreement with experiments (see Sec. III C). We remark that the experimental lattice thermal conductivities are always obtained from the total thermal conductivity and the subtraction of the electronic contribution by applying the Wiedemann-Franz law.

The thermal conductivity is strongly anisotropic due to the presence of weak Te-Te bonds between adjacent quintuple layers. The cumulative lattice thermal conductivity within the SMA of Sb_2Te_3 as a function of phonons frequency is shown in Fig. 10 along with average group velocities, phonon lifetimes, and mean free paths. The contribution of optical modes to the thermal conductivity is marginally more important for Sb_2Te_3 than for the GeTe, reaching here a contribution of 35%.

C. $Ge_2Sb_2Te_5$

The hexagonal phase of $Ge_2Sb_2Te_5$ has $P\bar{3}m_1$ symmetry and nine atoms per unit cell in nine layers stacked along the c axis. Two different sequences have been proposed, namely, the ordered stacking Te-Sb-Te-Ge-Te-Ge-Te-Sb-Te-Te-Sb- [17] shown in Fig. 11 (Kooi structure, named stacking A in Ref. [47] and hereafter) and the ordered stacking Te-Ge-Te-Sb-Te-Sb-Te-Ge-Te-Te-Ge- [18] (Petrov structure, named stacking B in Ref. [47] and hereafter). As already mentioned, recent diffraction measurements suggested, however, a disordered phase with Sb and Ge randomly occupying the same layers [19] (Matsunaga structure, named stacking C in Ref. [47] and hereafter) which is also confirmed by transmission electron microscopy imaging of GST nanowires [20]. The structure can be seen as a stacking of $Ge_2Sb_2Te_5$ quintuple layers with weak Te-Te bonds between adjacent layers.

In a previous work [47] we optimized the geometry of $Ge_2Sb_2Te_5$ in stackings A and B within DFT-PBE. We also modeled the disordered phase C by doubling the unit cell along the b axis and putting one Ge and one Sb atom on each Ge/Sb layer (18-atom supercell). The geometry chosen for stacking C corresponds to the best quasirandom structure compatible with an 18-atom supercell [48]. Stacking A is lower in energy than stacking B (by 19 meV/atom). Stacking C is only marginally higher in energy than stacking A, actually within the free-energy contribution expected for configurational disorder, and it is even marginally lower in energy than stacking A if

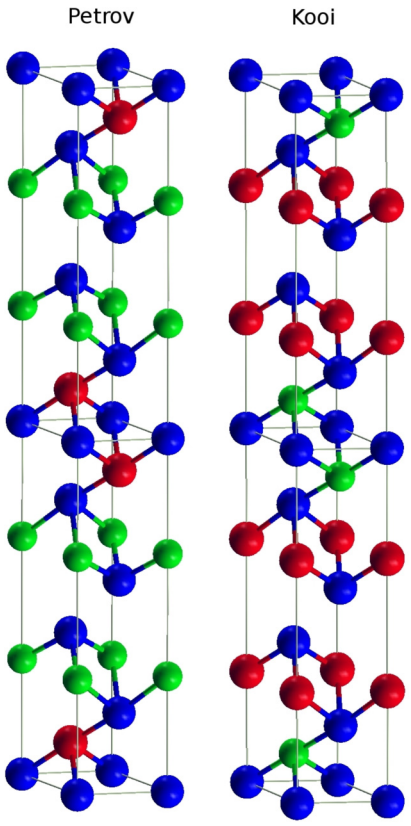

FIG. 11. Structure of $Ge_2Sb_2Te_5$ in the hexagonal cell in stacking A (Kooi) and B (Petrov). Two formula units along the c axis and period replica of atoms at the edges of the hexagonal cell in the ab plane are shown. Atoms independent by symmetry are labeled. In stacking A and B, the positions of Ge and Sb atoms are interchanged. The weak Te-Te bonds (3.7 Å long) connecting adjacent slabs are not shown to emphasize the presence of $Ge_2Sb_2Te_5$ stacks. Blue, green, and red spheres denote Te, Ge, and Sb atoms.

the hybrid B3PW functional [49] is used. The crystal structure of $Ge_2Sb_2Te_5$ in stacking A was optimized in Ref. [47] by constraining the $P\bar{3}m1$ crystal symmetry. This procedure was chosen because of the presence of an unstable optical phonon at the Γ point [47]. This instability is actually removed by adding a vdW interaction according to Grimme [26] as discussed in Ref. [50]. Therefore, the thermal conductivity has been computed here using the PBE functional supplemented by the vdW interaction of Ref. [26]. The equilibrium theoretical lattice parameters of $Ge_2Sb_2Te_5$ in stacking A and B obtained with the PBE functional with and without vdW corrections are compared with experimental data in Table IV. The BZ was sampled over a $8 \times 8 \times 8$ MP mesh for the self-consistent electron density.

GST is a degenerate p-type semiconductor as well with a hole density of about 2.73×10^{20} holes/cm^3 [51]. We consistently introduced holes (3×10^{20} holes/cm^3) compensated by a uniform background. The internal structure has been relaxed by fixing the lattice parameters to the values obtained without holes with negligible changes.

Phonon dispersion relations have been obtained by Fourier transforming the dynamical matrix computed on a $4 \times 4 \times 4$ MP grid in the BZ. Phonon dispersion relations are shown in Fig. 12 for the two stackings with and without vdW correction.

TABLE IV. Relative energies (meV/atom) and theoretical equilibrium lattice parameters (Å) for stacking A (Kooi) and B (Petrov) optimized with the PBE+vdW functional. Data without vdW corrections are reported in parentheses. The experimental data are from Refs. [17,19].

	Stacking		
	Kooi	Petrov	Exp.
Energy (meV/atom)	0 (0)	16 (19)	
	Cell parameters (Å)		
a	4.191 (4.28)	4.178 (4.25)	4.225[a]–4.25[b]
c	17.062 (17.31)	17.41 (17.74)	17.239[a]–17.27[b]

[a]Ref. [19].
[b]Ref. [17].

Anharmonic force constants have been computed following the same scheme used for GeTe and discussed in the previous sections. A $4 \times 4 \times 1$ q-point grid has been used. Fourier interpolation has been made over a $20 \times 20 \times 7$ grid with a smearing of 2 cm^{-1} for energy conservation.

The thermal conductivities at 300 K for the ordered $Ge_2Sb_2Te_5$ crystal in stacking A and B obtained from the full solution of the BTE with the PBE+vdW functional are reported in Table V compared with the SMA result, which is lower by less than 5% with respect to the value obtained from the full solution of the BTE. The average thermal conductivity of about 1.6–1.2 W m^{-1} K^{-1} is sizably larger than the experimental value of 0.45 W m^{-1} K^{-1} reported in Ref. [9].

The spectral functions [Eq. (2)] of GST in stacking A and B and including only anharmonic lifetimes are shown in Fig. 13. The cumulative lattice thermal conductivity within the SMA of $Ge_2Sb_2Te_5$ as a function of phonons frequency is shown for stacking A and B in the side columns of Fig. 14, along with group velocities, phonon lifetimes, and mean free paths averaged over a small energy window of 2 cm^{-1}.

We then introduced in the BTE the scattering due to vacancies in either the Sb or Ge sublattice with a concentration assigned by the holes density of 3×10^{20} holes/cm^3 close to the value measured by the Hall effect [51]. This holes density corresponds to either 1.8 at. % vacancies in the Ge sublattice (two holes per vacancy involving only electrons from p orbitals) or to 1.25 at. % vacancies in the Sb sublattice (three holes per vacancy). The average thermal conductivity is reduced to about 0.8–1.1 W m^{-1} K^{-1}(Table VI), which is still much higher than the experimental value. By increasing the vacancy concentration up to 3 at. % in the Ge sublattice, the average thermal conductivity is further reduced to 0.64–0.86 W m^{-1} K^{-1}.

To better model the experimental conditions, we have then introduced disorder in the Ge/Sb sublattice by adding an isotopic phonon scattering rate in the BTE (see Sec. II). By considering a full Ge/Sb mass mixing and neglecting Ge/Sb vacancies the average thermal conductivity is sizably reduced to 0.61–0.76 W m^{-1} K^{-1} (see Table VI). By further adding

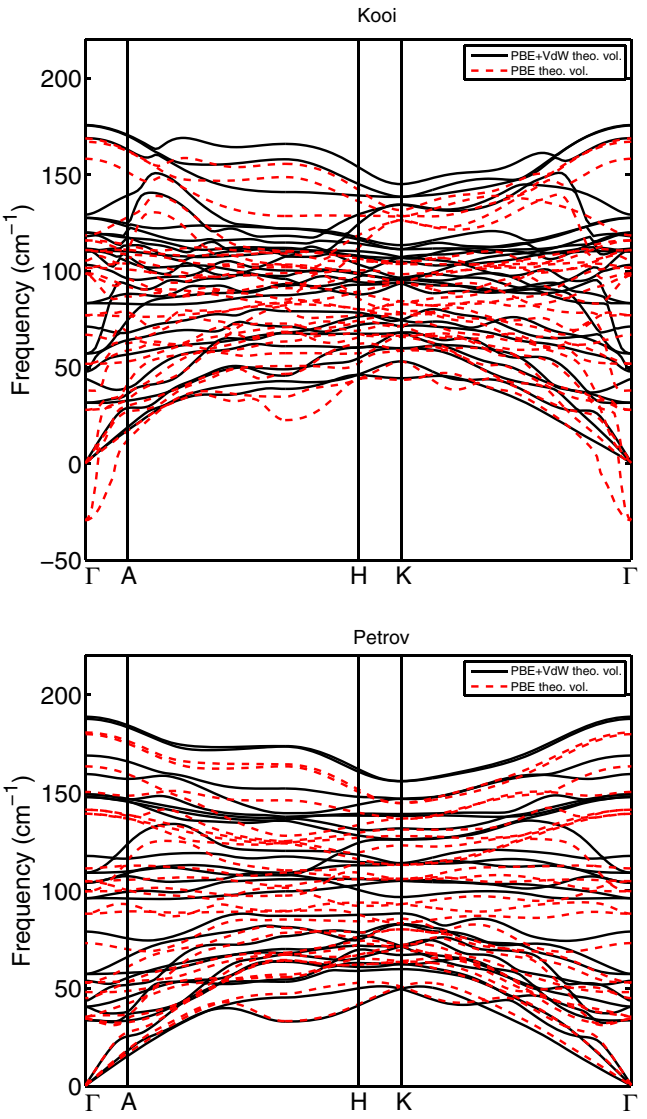

FIG. 12. Phonon dispersion relations of $Ge_2Sb_2Te_5$ for stacking A (Kooi) and B (Petrov) stackings from PBE and PBE+vdW calculations.

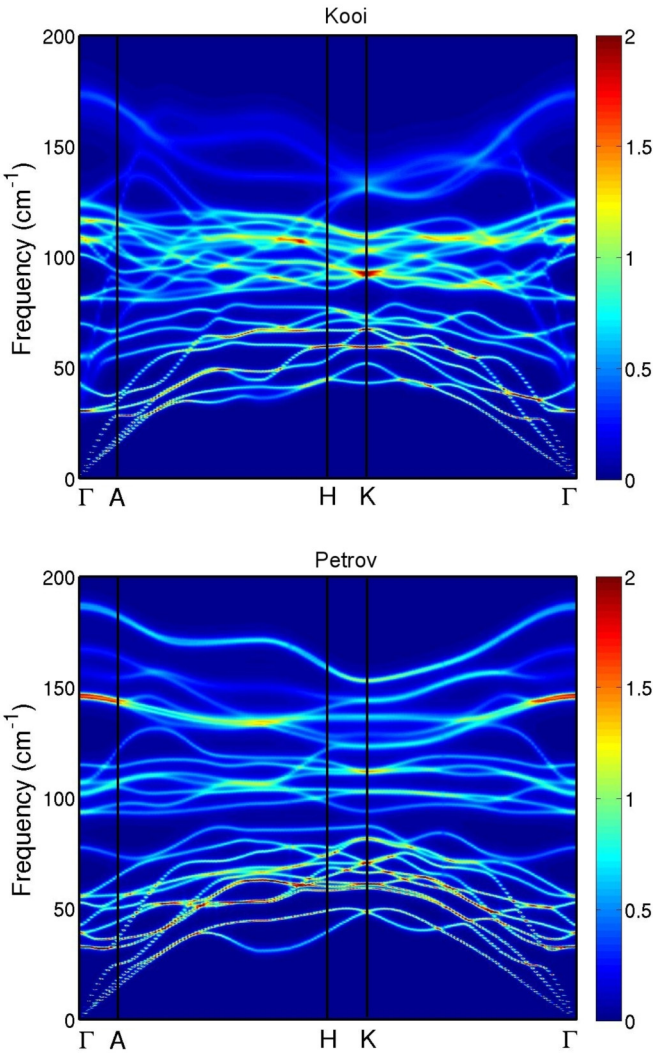

FIG. 13. Spectral function $\omega \cdot \sigma(\mathbf{q},\omega)$ [see Eq. (2)] of GST in the stacking A (Kooi) and B (Petrov) with anharmonic broadening only.

on top of Ge/Sb disorder the scattering due to 1.8 at. % Ge vacancies or 1.25 at. % Sb vacancies, the average thermal conductivity is further reduced to 0.43–0.58 W m^{-1} K^{-1} or 0.28–0.42 W m^{-1} K^{-1} (see Table VI).

TABLE V. Lattice thermal conductivity (W m^{-1} K^{-1}) of hexagonal $Ge_2Sb_2Te_5$ at 300 K along the c axis in the hexagonal notation (κ_z, see Fig. 11) in the perpendicular plane (κ_x) and their average for a polycrystalline sample (κ_{av}, see text). Both stacking A (Kooi) and B (Petrov) are considered. The thermal conductivity is computed for the perfect crystals using the exact variational solution of the BTE and within the SMA.

	Exact			SMA		
	κ_z	κ_x	κ_{av}	κ_z	κ_x	κ_{av}
Kooi	0.34	1.59	1.20	0.34	1.51	1.12
Petrov	0.59	2.10	1.60	0.58	2.00	1.53

The cumulative lattice thermal conductivity within the SMA of $Ge_2Sb_2Te_5$ as a function of phonons frequency is shown in the central column of Fig. 14 for stacking B by including Sb/Ge disorder (Matsunaga model) and vacancies in the Sb sublattice. Group velocities, phonon lifetimes, and mean free paths averaged over a small energy window of 2 cm^{-1} are also shown in the same figure. The temperature dependence of the thermal conductivity for this latter system averaged over the three Cartesian directions is shown in Fig. 15.

From Figs. 13 and 14 it is clear that the acoustic phonons mostly contribute to the thermal conductivity at 300 K, with a small contribution from the lower-energy optical modes and a negligible contribution from the high-energy optical modes. In the disordered Matsunaga phase in particular, the whole lattice thermal conductivity originates from the acoustic modes with energy below 30 cm^{-1}.

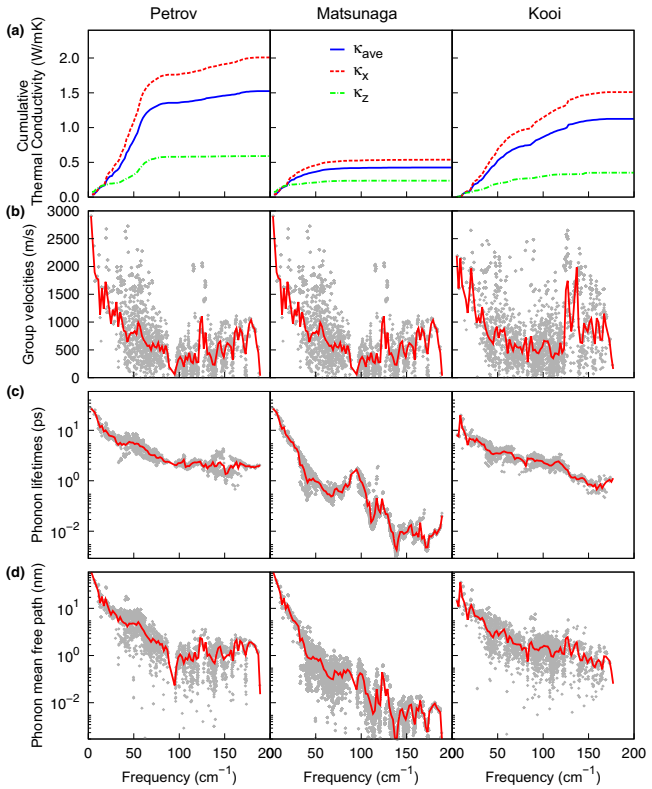

FIG. 14. (a) Cumulative lattice thermal conductivities within the SMA (see text) along the c axis in the hexagonal notation (κ_z, see Fig. 1) in the perpendicular plane (κ_x) and their average for a polycrystalline sample (κ_{av}, see text), (b) group velocities, (c) phonon lifetimes, and (d) mean free paths over a small energy window of 2 cm^{-1} as a function of phonon frequencies in $Ge_2Sb_2Te_5$ crystal at 300 K for stacking A (Kooi, right panels), B (Petrov, left panels), and for the disordered stacking according to Matsunaga (central panels) including vacancies (see text).

TABLE VI. Lattice thermal conductivity of hexagonal $Ge_2Sb_2Te_5$ at 300 K along the c axis in the hexagonal notation (κ_z, see Fig. 11) in the perpendicular plane (κ_x) and their average for a polycrystalline sample (κ_{av}, see text). Both stacking A (Kooi) and B (Petrov) are considered. The thermal conductivity is computed for the perfect crystals (ideal), for a crystal with 1.8 at. % of Ge vacancies (1.8% Ge vac, see text), for 1.25 at. % of Sb vacancies (1.25% Sb vac, see text), for a complete disorder in the Ge/Sb sublattice with no vacancies (Ge/Sb disorder, Matsunaga structure), and finally with both disorder in the Ge/Sb and a content of Ge vacancies (Ge/Sb + Ge vac) or Sb vacancies (Ge/Sb + Sb vac) as given above. All the results refer to the exact BTE solution, however the differences between exact and SMA results are marginal. Data are given in $W\,m^{-1}\,K^{-1}$. The experimental [9] lattice thermal conductivity is 0.45 $W\,m^{-1}\,K^{-1}$.

	A (Kooi)			B (Petrov)		
	κ_z	κ_x	κ_{av}	κ_z	κ_x	κ_{av}
Ideal	0.34	1.59	1.20	0.59	2.10	1.60
1.8% Ge vac	0.28	1.19	0.83	0.42	1.49	1.13
1.25% Sb vac	0.25	1.10	0.82	0.47	1.50	1.16
Ge/Sb disorder	0.20	0.77	0.61	0.30	0.99	0.76
Ge/Sb + Ge vac	0.16	0.56	0.43	0.25	0.75	0.58
Ge/Sb + Sb vac	0.11	0.37	0.28	0.23	0.51	0.42

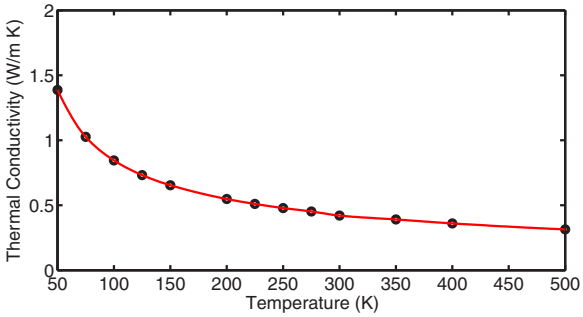

FIG. 15. Temperature dependence of thermal conductivity of polycrystalline GST with disorder in the Sb/Ge sublattice and including vacancies (see text).

Note that disordering the Kooi or Petrov structures with a 50-50 occupation by Sb and Ge in all layers leads to the same structure and thus in principle to the same lattice thermal conductivity. This is not the case for the results in Table IV because disorder has been introduced perturbatively. This approximation leads to a dependence of the final results on the choice of the ordered starting configuration. In the structural model proposed by Matsunaga, the disorder in the occupation of the Ge/Sb sites is actually not complete as the cationic lattice sites closer to the vdW gap are occupied by Sb in a fraction of 56% (with a reversed proportion for the inner cationic sites). The uncertainties related to our perturbative approach to the disorder prevent us from assessing such small deviations from a 50-50 occupation of the Sb/Ge sites on the basis of the calculated thermal conductivity. In spite of these uncertainties, it is clear that both vacancies and disorder are needed to achieve a good agreement between theoretical and experimental data (see Table VI). This result strongly suggests that the low thermal conductivity in the hexagonal phase of GST is actually an indicator of the (Ge/Sb) sublattice disorder confirmed by recent experimental data from Z-resolved TEM in GST nanowires [20].

We remark that the thermal conductivity was obtained from the solution of the BTE with the inclusion of disorder in the Sb/Ge sublattice and vacancies in $Ge_2Sb_2Te_5$. The value of 0.42 $W\,m^{-1}\,K^{-1}$ in Table VI is very close to the minimum thermal conductivity obtained from the theoretical average transverse and longitudinal sound velocity (v_L, v_T) and atomic density n_a according to Cahill *et al.* [52] and valid above the Debye temperature as given by

$$\kappa_{\min} = \frac{1}{2}\left(\frac{\pi n_a^2}{6}\right)^{\frac{1}{3}}(v_L + 2v_T)k_B \qquad (3)$$

where k_B is the Boltzmann constant. By plugging in Eq. (3) the sound velocities averaged over the BZ $v_L = 3120$ m/s and v_T=1950 m/s one finds $\kappa_{\min} = 0.43\,W\,m^{-1}\,K^{-1}$, which is close to the full DFT solution and to the experimental value of 0.45 $W\,m^{-1}\,K^{-1}$ as already observed in Refs. [9,53]. This result raises an overall concern on the applicability of the BTE itself in the presence of such a strong phonon scattering due to disorder. However, as we can see in Fig. 14, disorder does not affect the phonon mean free path in the same manner for all

frequencies. The disorder actually suppresses the contribution to the thermal conductivity of phonons with frequency above 50 cm^{-1} which gives instead an important contribution to the thermal conductivity of the ideal crystal. On the other hand phonons with frequency below 30 cm^{-1} that mostly contribute to the thermal conductivity of the disordered crystal still show a mean free path of several nm which seems consistent with the use of a BTE approach.

Note that the lattice thermal conductivity of GeTe, Sb_2Te_3, and $Ge_2Sb_2Te_5$ has been computed by using the anharmonic force constant computed at 0 K. In a recent theoretical paper [54] on the lattice thermal conductivity of Bi_2Te_3 which is isostructural and isoelectronic with Sb_2Te_3, it is shown that the lattice expansion has little effect on anharmonic force constants. On the other hand, it is shown that the effects of thermal phonon population on the anharmonic force constants are not negligible in Bi_2Te_3 at 300 K. The use of the anharmonic force constants obtained at 0 K leads to an underestimation of about 20% of the in-plane lattice thermal conductivity at 300 K with respect to the value obtained with the anharmonic force constant extracted consistently from molecular-dynamics simulations at 300 K [54]. It remains to be seen whether a similar effect might be present in GeTe, Sb_2Te_3, and $Ge_2Sb_2Te_5$ compounds. If this were the case, the error introduced by the use made here of the 0-K anharmonic force constants would not change anyway our conclusions on the need of introducing defects either in the form of vacancies (in GeTe) or disorder in the occupation of the Sb/Ge sublattices (in GST) to reproduce the experimental lattice thermal conductivity.

IV. CONCLUSIONS

We have computed the lattice thermal conductivity of the phase change compound $Ge_2Sb_2Te_5$ in the hexagonal crystalline phase from the full solution of the linearized Boltzmann transport equation with phonons and phonon-phonon scattering rates computed within density functional perturbation theory. Due to the weak Te-Te bonds, the lattice thermal conductivity is strongly anisotropic with a low conductivity along the c axis. However, scattering due to disorder in the Sb/Ge sublattice has to be introduced to bring the thermal conductivity close to the value of 0.45 $W\,m^{-1}\,K^{-1}$ measured experimentally. These results confirm the presence of disorder in the Sb/Ge sublattices emerged from most recent x-ray-diffraction data [19] and from transmission electron microscopy of nanowires [20]. The same calculations on the GeTe trigonal crystal reveal that the presence of Ge vacancies, responsible for a degenerate p-type character, leads to the large variability of the bulk thermal conductivity measured experimentally for this compound. A similarly good agreement with experiments is obtained for the thermal conductivity of Sb_2Te_3.

ACKNOWLEDGMENTS

M.B. acknowledges funding from the European Union Seventh Framework Programme FP7/2007-2013 under Grant No. 310339 and computational resources provided by Cineca (Casalecchio di Reno, Italy) through the ISCRA initiative. L.P. and F.M. acknowledge funding from DARI, Dossier No. 2015097320.

[1] M. Wuttig and N. Yamada, Nat. Mater. **6**, 824 (2007).
[2] A. Pirovano, A. L. Lacaita, A. Benvenuti, F. Pellizzer, and R. Bez, IEEE Trans. Electron. Dev. **51**, 452 (2004).
[3] A. L. Lacaita and D. J. Wouters, Phys. Status Solidi A **205**, 2281 (2008).
[4] D. Lencer, M. Salinga, and M. Wuttig, Adv. Mat. **23**, 2030 (2011).
[5] S. Raoux, W. Welnic, and D. Ielmini, Chem. Rev. **110**, 240 (2010).
[6] J. P. Reifenberg, D. L. Kencke, and K. E. Goodson, IEEE Electron Device Lett. **29**, 1112 (2008).
[7] E. Bozorg-Grayeli, J. P. Reifenberg, M. Asheghi, H.-S. P. Wong, and K. E. Goodson, Ann. Rev. Heat Transfer **16**, 397 (2013).
[8] K. S. Siegert, F. R. L. Lange, E. R. Sittner, H. Volker, C. Schlockermann, T. Siegrist, and M. Wuttig, Rep. Prog. Phys. **78**, 013001 (2015).
[9] J. Lee, E. Bozorg-Grayeli, S. B. Kim, M. Asheghi, P. H.-S. Wong, and K. E. Goodson, Appl. Phys. Lett. **102**, 191911 (2013).
[10] R. Fallica, E. Varesi, L. Fumagalli, S. Spadoni, and M. Longo, Phys. Status Solidi RRL **7**, 1107 (2013).
[11] L. E. Shelimova, O. G. Karpinskii, P. P. Konstantinov, M. A. Kretova, E. S. Avilov, and V. S. Zemskov, Inorg. Mater. **37**, 342 (2001).
[12] P. Nath and K. L. Chopra, Phys. Rev. B **10**, 3412 (1974).
[13] R. Lan, R. Endo, M. Kuwahara, Y. Kobayashi, and M. Susa, J. Appl. Phys. **112**, 053712 (2012).
[14] J. M. Yanez-Limon, J. Gonzalez-Hernandez, J. J. Alvarado-Gil, I. Delgadillo, and H. Vargas, Phys. Rev. B **52**, 16321 (1995).
[15] D. H. Damon, M. S. Lubell, and R. Mazelsky, J. Phys. Chem. Solids **28**, 520 (1967).
[16] K. Yokota and S. Katayama, Jpn. J. Appl. Phys. **12**, 1205 (1973).
[17] B. J. Kooi and T. M. J. De Hosson, J. Appl. Phys. **92**, 3584 (2002).
[18] I. I. Petrov, R. M. Imanov, and Z. G. Pinsker, Sov. Phys. Crystallogr. **13**, 339 (1968).
[19] T. Matsunaga, N. Yamada, and Y. Kubota, Acta Crystallogr. B **60**, 685 (2004).
[20] E. Rotunno, L. Lazzarini, M. Longo, and V. Grillo, Nanoscale **5**, 1557 (2013).
[21] S. Baroni, S. de Gironcoli, and A. Dal Corso, Rev. Mod. Phys. **73**, 515 (2001).
[22] L. Paulatto, F. Mauri, and M. Lazzeri, Phys. Rev. B **87**, 214303 (2013).
[23] G. Fugallo, M. Lazzeri, L. Paulatto, and F. Mauri, Phys. Rev. B **88**, 045430 (2013).
[24] P. Giannozzi *et al.*, J. Phys.: Condens. Matter **21**, 395502 (2009); www.quantum-espresso.org.
[25] J. P. Perdew, K. Burke, and M. Ernzerhof, Phys. Rev. Lett. **77**, 3865 (1996).
[26] S. Grimme, J. Comput. Chem. **27**, 1787 (2006).

[27] R. Shaltaf, X. Gonze, M. Cardona, R. K. Kremer, and G. Siegle, Phys. Rev. B **79**, 075204 (2009).
[28] H. Monkhorst and J. D. Pack, Phys. Rev. B **13**, 5188 (1976).
[29] A. Debernardi, S. Baroni, and E. Molinari, Phys. Rev. Lett. **75**, 1819 (1995); M. Lazzeri and S. de Gironcoli, Phys. Rev. B **65**, 245402 (2002); G. Deinzer, G. Birner, and D. Strauch, *ibid.* **67**, 144304 (2003).
[30] M. Omini and A. Sparavigna, Il Nuovo Cimento **19D**, 1537 (1997).
[31] C. A. Ratsifaritana and P. G. Klemens, Int. J. Thermophys. **8**, 737 (1987).
[32] D. Campi, D. Donadio, G. C. Sosso, J. Behler, and M. Bernasconi, J. Appl. Phys. **117**, 015304 (2015).
[33] J. Goldak, C. S. Barrett, D. Innes, and W. Youdelis, J. Chem. Phys. **44**, 3323 (1966).
[34] T. Chatterji, C. M. N. Kumar, and U. D. Wdowik, Phys. Rev. B **91**, 054110 (2015).
[35] G. Lucovsky and R. M. White, Phys. Rev. B **8**, 660 (1973).
[36] T. Chattopadhyay, J. Boucherle, and H. Von Schnering, J. Phys. C **20**, 1431 (1987).
[37] K. Shportko, S. Kremers, M. Woda, D. Lencer, J. Robertson, and M. Wuttig, Nat. Mater. **7**, 653 (2008); D. Lencer, M. Salinga, B. Grabowski, T. Hickel, J. Neugebauer, and M. Wuttig, *ibid.* **7**, 972 (2008); B. Huang and J. Robertson, Phys. Rev. B **81**, 081204(R) (2010).
[38] A. H. Edwards, A. C. Pineda, P. A. Schultz, M. G. Martin, A. P. Thompson, H. P. Hjalmarson, and C. J. Umrigar, Phys. Rev. B **73**, 045210 (2006).
[39] A. J. Bevolo, H. R. Shanks, and D. E. Eckels, Phys. Rev. B **13**, 3523 (1976).
[40] M. Methfessel and A. T. Paxton, Phys. Rev. B **40**, 3616 (1989).
[41] L. Paulatto, I. Errea, M. Calandra, and F. Mauri, Phys. Rev. B **91**, 054304 (2015).
[42] T. L. Anderson and H. B. Krause, Acta Crystallogr. B **30**, 1307 (1974).
[43] Y. Ma, G. Liu, P. Zhu, H. Wang, X. Wang, Q. Cui, J. Liu, and Y. Ma, J. Phys.: Condens. Matter **24**, 475403 (2012).
[44] G. C. Sosso, G. Miceli, S. Caravati, J. Behler, and M. Bernasconi, Phys. Rev. B **85**, 174103 (2012).
[45] G. C. Sosso, S. Caravati, and M. Bernasconi, J. Phys.: Condens. Matter **21**, 095410 (2009).
[46] *Non-Tetrahedrally Bonded Elements and Binary Compounds I*, edited by O. Madelung, U. Rössler, and M. Schulz, Landolt-Börnstein - Group III Condensed Matter, Vol. 41C (Spinger-Verlag, Heidelberg, 1998), pp. 1–5.
[47] G. C. Sosso, S. Caravati, C. Gatti, S. Assoni, and M. Bernasconi, J. Phys.: Condens. Matter **21**, 245401 (2009).
[48] A. Zunger, S.-H. Wei, L. G. Ferreira, and J. E. Bernard, Phys. Rev. Lett. **65**, 353 (1990).
[49] A. D. Becke, J. Chem. Phys. **98**, 5648 (1993); J. P. Perdew and Y. Wang, Phys. Rev. B **45**, 13244 (1992).
[50] D. Campi, E. Baldi, G. Graceffa, G. C. Sosso, and M. Bernasconi, J. Phys.: Condens. Matter **27**, 175009 (2015).
[51] B.-S. Lee, J. R. Abelson, S. G. Bishop, D.-H. Kang, B.-K. Cheong, and K.-B. Kim, J. Appl. Phys. **97**, 093509 (2005).
[52] D. G. Cahill, S. K. Watson, and R. O. Pohl, Phys. Rev. B **46**, 6131 (1992).
[53] T. Tsafack, E. Piccinini, B.-S. Lee, E. Pop, and M. Rudan, J. Appl. Phys. **110**, 063716 (2011).
[54] O. Hellman and D. A. Broido, Phys. Rev. B **90**, 134309 (2014).